14.4

MESOSCALE ENVIRONMENTS WHICH CHARACTERIZE SEVERE MID-UPPER TROPOSPHERIC TURBULENCE

M. L. Kaplan, Y. L. Lin, J. J. Charney, K. T. Waight III*, A. W. Huffman, J. D. Cetola, and K. M. Lux
Department of Marine, Earth, and Atmospheric Sciences
North Carolina State University
Raleigh, North Carolina 27695-8208
*MESO Inc.
1005 Capability Drive
Raleigh, North Carolina 27695

1. INTRODUCTION

In a recent study, Kaplan et al. (2000a) described the synoptic/meso-alpha scale environment that characterized the period immediately preceding convective turbulence. The main features in the environment included: 1) the entrance region of an upper tropospheric jet stream, 2) very distinct curvature in the upstream wind and pressure field, 3) nearby convection, 4) low relative vorticity, 5) upward vertical motion, and 6) cold advection. In this paper we will focus the dynamical analyses described in the previous study to finer scales of motion such that it specifies the meso-beta/meso-gamma scale precursor processes to both clear air and convective turbulence. These processes are the logical extension of the meso-alpha scale environment findings in that they are focused on the mechanism for significant accelerations, convergence of vorticity, and decreasing Richardson number. We will employ mesoscale numerical model simulations from a hydrostatic and a nonhydrostatic model to synthesize a theory for how meso-beta/gamma scale circulations organize an environment conducive to intense vortex formation as well as how these processes can be combined into a single predictive index. This predictive index is based on the concept that the time tendency of enstrophy is a very powerful indicator of the potential for turbulence to develop. Fine-scale vortices exist where enstrophy tendencies maximize and shearing instability is probable. The environment conducive to turbulence is one that supports UNBALANCED SUPERGRADIENT FLOW.

2. NUMERICAL MODEL AND CASE STUDIES

The numerical models to be utilized in the following analyses are the hydrostatic and nonhydrostatic version of the Mesoscale Atmospheric Simulation System (MASS), i.e., versions 5.13 (HMASS) and 6.0 (NHMASS), respectively. Details of HMASS can be found in Kaplan et al. (2000b). NHMASS employs a turbulence kinetic energy (TKE) planetary boundary layer scheme. Both versions include the Kain-Fritsch cumulus parameterization scheme, grid scale precipitation, and conservation equations for cloud water, rainwater, ice, and snow. Four case studies will be analyzed including one clear air case study employing a 6-km horizontal resolution using HMASS and three convective turbulence events using NHMASS with 2-km, 500-m and finer horizontal resolution. Initial conditions and lateral boundary conditions for each coarse mesh simulation are derived from the NWS ETA analyses and initial and lateral boundary conditions for each nested-grid simulation are derived from each successively coarser simulation. All four case studies are examples of extreme turbulence events either observed during field experiment studies or commercial airline flights.

3. BASIC TURBULENCE PARADIGM

The fundamental assumptions inherent in the paradigm illustrated in the four case study simulations include:

a) unbalanced supergradient flow in proximity to thermal advection and/or differential diabatic heating creates environment favorable for severe turbulence,
b) enstrophy tendency maxima and turbulence probability are highly correlated,
c) regions of maxima in the gradient of Montgomery stream function on an isentrope (pressure gradient force), which are orthogonal to regions of maxima in the gradients of relative vorticity, have a maxima in the cross-product, and are most favorable for turbulence exhibiting units equivalent to enstrophy tendency,
d) these regions are locations of substantial separation between the geostrophic vorticity maxima and the total vorticity maxima, hence, they are highly accelerative and are regions where increasing accelerative flow is accompanied by diminishing values of Richardson number,
e) regions are coincident to maxima in the time tendency in the convergence of absolute vorticity on isentropic surfaces,
f) the region of maxima in the convergence of absolute vorticity on a sloping isentrope is also a region of minima in Richardson number within the layer as separation of the isentropes in the vertical and vertical variation of increasing wind velocity maximize where the isentrope slope is greatest.

This index (i.e., the cross product of the gradient of the Montgomery stream function and the gradient of the relative vorticity) synthesizes both rotation and vertical buoyancy/shear into a single term. This synergy occurs when the acceleration vector is orthogonal to relative vorticity gradients on isentropic surfaces, hence, parcels are converging relative vorticity into regions of simultaneously decreasing Richardson number. The assumption is that fine scale shearing instability and increasing vorticity in the same place and time are critical to severe turbulence. This is consistent with recent studies of Clark et al. (2000), Andreassen et al. (1998), and Fritts et al. (1998). Past studies of turbulence forecast indices have focused on Richardson number (Uccellini et al. 1986), Richardson number tendency (Keller 1990), and deformation multiplied by vertical wind shear (Ellrod and Knapp 1992). They have focused on the role of buoyancy, vertical shear, and/or horizontal frontogenetic forcing in reducing the Richardson number INDEPENDENT OF ROTATION. In this study, the turbulence predictive index is not independent of Richardson number or rotation and is maximized where the acceleration vector is acting to increase the importance of BOTH processes. This occurs where supergradient wind flow is prolonged by the appropriate configuration of the pressure gradient force. This is consistent with Knox's (1997) study on the role of inertial instability in CAT formation with the caveat that the thermal distribution helps sustain supergradient wind flow thus accentuating the probability for the maximization of the curl of the Montgomery stream function and relative vorticity on an isentrope.

4. SIMULATIONS DEPICTING THE PARADIGM

Clear Air Case Study/Meso-Beta Scale Analyses

Figure 1 depicts the hydrostatic 6 km simulated 313K (~420 mb) winds and relative vorticity for the Cape Girardeau turbulence accident case study at 1230 UTC. The 6-km hydrostatic MASS simulation was nested within a 30-km simulation initialized at 0000 UTC 28 January while the 6-km simulation was initialized at 0600 UTC 28 January. This accident occurred near this level shortly after 1445 UTC approximately 80 km southwest of Farmington, Missouri (northwest of the Missouri boot heel). The simulation shows the confluence of the entrance regions of the subtropical jet (STJ) and polar jet (PJ) as well as curved flow near the accident location. Within this region of confluent flow, the curvature and shears produce a very strong gradient of relative vorticity from NW-SE over the accident location (i.e., relative vorticity contours oriented WSW-ENE). The relatively cold air to the north-northeast and warm air to the south-southwest insures that the column thickness tilts the Montgomery stream function (M) from SSW-NNE reflecting the cyclonically curved synoptic flow regime. This produces a maximum in the gradient of M oriented towards the north-northeast, nearly orthogonal to the gradient of relative vorticity. This results in a maximum in the curl of these two quantities, as depicted in Figure 2. The location of the maximum is very close to the accident location and coincident with the strongest supergradient wind flow over southeastern Missouri and extreme southwestern Kentucky where the centripetal and pressure gradient force contributions to the air motion overwhelm the inertial contribution. This is also a region of negative Richardson number advection and, hence a region of downfolding isentropes in proximity to increasing convergence times vorticity (not shown).

Convective Case Studies/Meso-Beta and Meso-Gamma Scale Analyses

Wilmington, Delaware Case study

This turbulence case study differs from the previous case study in two ways: 1) the turbulence accident occurs in the mid-troposphere near 775 mb and 2) moist convection unambiguously contributes to the dynamics. The severe turbulence was observed approximately 50 km south-southeast of Wilmington, Delaware shortly after 1930 UTC 13 January 2000. Figure 3 shows wind and absolute vorticity on the 285K isentrope at 1930 UTC, diagnosed from the 2-km NHMASS model simulation. The 2-km nonhydrostatic simulation was nested within the 6 km hydrostatic simulation which was nested within an 15-km hydrostatic simulation at 1900 UTC, 1200 UTC, and 0000 UTC 13 January, respectively. As in the Cape Girardeau case, intersecting jets are in place in proximity to curved flow. However, synoptic jets and mesoscale jetlets can both be seen. One mesoscale jetlet, comprised of west-northwesterly momentum, originates from upstream gap flow within the break in the Appalachians in western Maryland. A second mesoscale jetlet, comprised of predominantly southwesterly flow, originates from the pressure ridge that forms along the lee slope of the Blue Ridge Mountains of western Virginia. Diabatic heating and surface sensible heat flux have produced this thermal ridge, which acts to accelerate the flow towards the northeast. These jetlets are embedded within highly curved synoptic jets in the northwesterly flow over the Delaware Valley region. These features, in concert with a cold cyclonic trough and its accompanying cold air advection in the synoptic scale flow, frame the environment after 1830 UTC south-southeast of Wilmington, Delaware in the lower-middle troposphere. Figure 4a depicts the vorticity after the development of a line of convection after 2030 UTC over southwestern New Jersey. The evolving flow accompanying increasing curvature coupled with the development of convection over southwestern New Jersey act to create a change in vorticity structure such that the original nearly W-E orientation shifts to NW-SE. At the same time, the gradient of M shifts from W-E reflecting the NE-SW cold advection as the convection produces a mesoscale ridge perturbation of M imbedded within the larger region of cold advection (Fig. 4b). The isentropic surfaces reflect the downfolding and convergence of vorticity as both cold advection and latent heating (not shown) perturb the 285K surface. This case was nested to 500-m horizontal resolution at 1930 UTC and to 125-m horizontal resolution at 2045 UTC. As the scale is reduced, the vorticity field and downfolding of the isentropes intensify as a meso-gamma scale outflow jet develops close to the location of the accident (depicted in Figure 5).

Valdosta, Georgia Case Study

This case study reflects a very strong observation of turbulence during a NASA B-757 turbulence flight experiment. The observation ~50 km southwest of Valdosta, Georgia at ~1845 UTC 14 December 2000 at ~33,000 feet. Figure 6 depicts the 334K winds and absolute vorticity accompanying a 2 km nonhydrostatic MASS simulation valid at 1845 UTC which was nested within a 6 km and 30 km HMASS simulation which were initialized at 1830 UTC, 1200 UTC, and 0000 UTC 14 December. The main meso-alpha scale jets are a west-southwesterly wind maximum over northern Georgia and a south-southwesterly wind maximum southwest of the Florida panhandle embedded within a trough while a meso-gamma scale convective jetlet can be seen near the accident location in Figure 6. The vorticity field in Figure 6 indicates that near the transition from positive to negative absolute vorticity over southern Georgia at the meso-beta scale is a meso-gamma scale vorticity gradient accompanying the convection and its outflow jetlet which is oriented SW-NE. Figure 7 depicts the value of M and its gradient, which indicates a nearly W-E orientation of the convectively generated M gradient, which is different from the larger-scale SW-NE oriented M gradient. Hence, the latent heating produces enough of a perturbation to the synoptic scale thickness gradient that the centripetal acceleration and pressure gradient force are pointing in the same direction. This results in an intersection of the M gradient vector and the vorticity gradient vector on the 334K isentrope as shown in Figure 8.

Cross City, Florida Case Study

A turbulence accident occurred at approximately 0045 UTC 2 October 1997 just southwest of Cross City, Florida at ~33,000 feet. There is every indication from satellite imagery that the turbulence event accompanied the development of a new convective cell on the northeastern flank of a previous long-lived small mesoscale convective system that had propagated across the southern part of Appalachee Bay. Figure 9 depicts the 0130 UTC 2 km simulated meso-alpha-beta scale winds and relative vorticity on the 335K surface which is located just below the level of the accident. The 2 km simulation was initialized from a 6 km and 18 km hydrostatic simulation initialized at 0000 UTC and 2230 UTC 1 October. The synoptic scale west-northwesterly flow and west-southwesterly flow is evident over the western Florida panhandle and northwestern Florida peninsula. These frame the multiple convective outflow jetlets over the south-central and eastern parts of Appalachee Bay. The alternating plumes of positive and negative relative vorticity maxima extending ENE towards the Florida coast near Cross City and covering the accident location produce ENE-oriented gradients of relative vorticity which intersect the convective heating-induced ESE-oriented gradients of Montgomery stream function, shown in Figure 10. This results in several very intense maxima of the turbulence index where the M and vorticity gradient vectors intersect between Cross City and the south-central Appalachee Bay, as shown in Figure 11.

5. SUMMARY AND CONCLUSIONS

We have employed multiscale numerical model simulations for four different severe turbulence case studies to illustrate a paradigm that characterizes the mesoscale and microscale environment prior to severe clear air and convective turbulence. The dynamical process that is the key organizing factor for all environments is unbalanced supergradient flow. The highly curved flow regime is the result of cold advection, intersecting wind maxima, and/or convective outflow jetlets. Once the centripetal acceleration becomes large in proximity to a rotated pressure gradient force vector, i.e., one which is oriented towards the direction of parcel motion, the inertial term in the equations of motion is incapable of decelerating the flow. This is manifested as large values of the cross product of the gradient of M and gradient of vorticity on an isentrope as well as the local time tendency of convergence times vorticity on an isentrope resulting in significant local time tendencies of enstrophy.

Acknowledgements

This research was supported by the NASA Langley Research Center under Contract #NAS1-99074 and Subcontract#82U-7473-008 to the Research Triangle Institute. The authors wish to thank Dr. Fred H. Proctor, the NASA Technical Contract Manager, as well as C. J. O'connor, the NASA-Langley Turbulence Characterization Program Manager, for their support.

References

Andreassen, O., P. O. Hvidsen, D. C. Fritts, and S. Arendt, 1998: Vorticity dynamics in a breaking internal gravity wave. Part 1. Initial instability evolution. J. Fluid. Mech., 367, 27-46.

Clark, T. L., W. D. Hall, R. M. Kerr, D. Middleton, L. Radke, F. Martin, Ralph, P. J. Nieman, and D. Levinson. 2000: Origins of aircraft-damaging clear air turbulence during the 9 December 1992 Colorado downslope windstorm: Numerical simulations and comparison to observations. J. Atmos. Sci., 57, 1105-1131.

Ellrod, G. P., and D. I. Knapp, 1992: An objective clear-air turbulence forecasting technique: verification and operational use. Wea. Forecasting, 7, 150-165.

Fritts, D. C., S. Arendt, and O. Andreassen, 1992: Vortex dynamics in a breaking internal gravity wave. Part 2. Vortex interactions and transition to turbulence. J. Fluid. Mech., 367, 47-65.

Kaplan, M. L., Y.-L. Lin, A. J. Riordan, K. M. Lux and A. W. Huffman, 2000a: Observational and numerical simulation-derived factors that characterize turbulence accident environments. Preprints, 9th AMS Conf. on Aerospace, Range, and Aeronautical Meteorology, 11-15 September 2000, Orlando, FL, 476-481.

-----------------, -----------, J. J. Charney, K. D. Pfeiffer, D. B. Ensley, D. S. DeCroix, and R. P. Weglarz, 2000b: A terminal area PBL prediction system at Dallas-Fort Worth and its application in simulating diurnal PBL jets. Bull. Amer. Meteor. Soc., 81, 2179-2204.

Keller, J. L., Clear air turbulence as a response to meso and synoptic-scale dynamical processes. Mon. Wea. Rev., 2228-2242.

Knox, J. A., 1997: Possible mechanisms of clear air turbulence in strongly anticyclonic flows. Mon. Wea. Rev., 125, 1251-1259.

Uccellini, L. W., K. F. Brill, R. A. Petersen, D. Keyser, R. Aune, P. J. Kocin, and M. des Jardins,: 1986: A report on the upper-level wind conditions preceding and during the Shuttle Challenger (STS 51L) explosion. Bull. Amer. Meteor. Soc., 67,1248-1265.

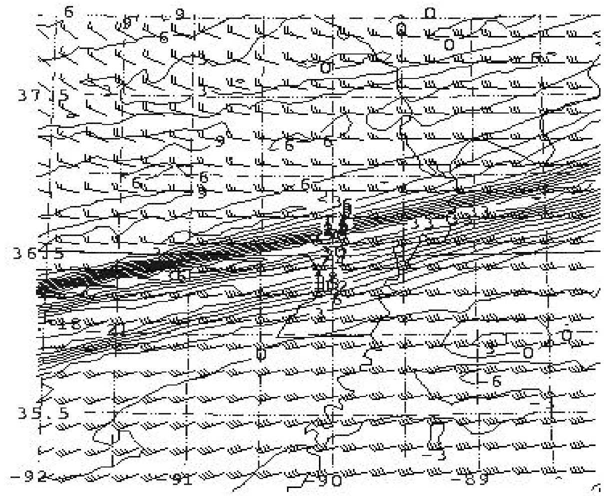

Figure 1. HMASS simulated 6 km 313K wind barbs (ms^{-1}) and relative vorticity (s^{-1} x 10^{-4}) for the Cape Girardeau, Missouri case valid at 1230 UTC 28 January 1997.

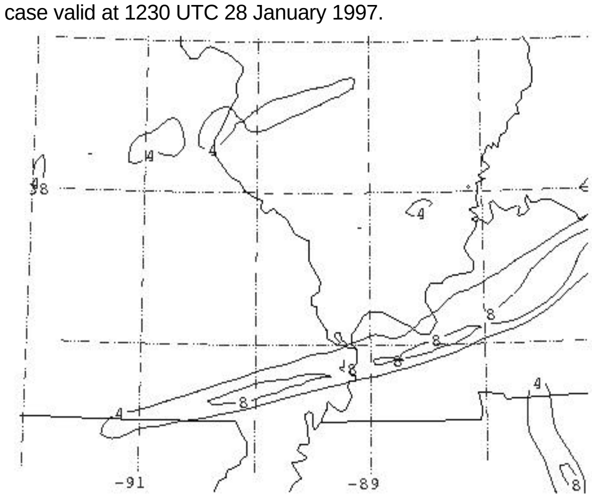

Figure 2. HMASS simulated 6 km 313K positive values of the cross-product of the gradient of M and the gradient of the relative vorticity (s^{-3} x 10^{-8}) for the Cape Girardeau, Missouri case valid at 1230 UTC 28 January 1997.

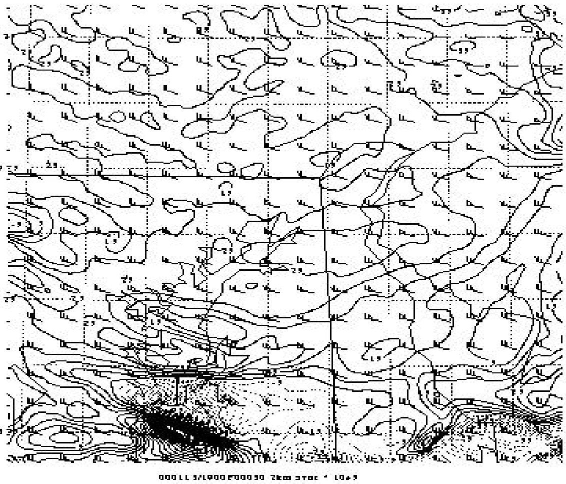

Figure 3. NHMASS simulated 2 km 285K wind barbs (ms^{-1}) and absolute vorticity ($s^{-1} \times 10^{-4}$) for the Wilmington, Delaware case valid at 1930 UTC 13 January 2000.

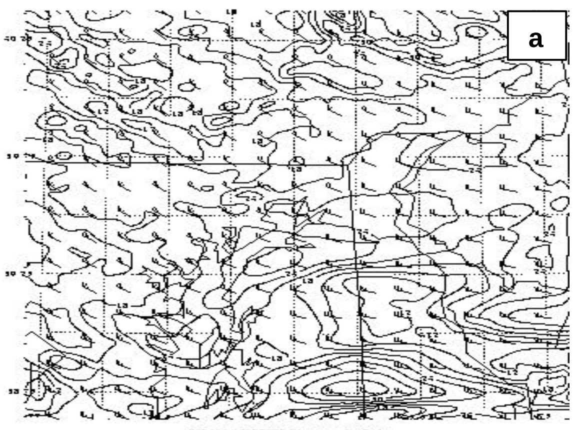

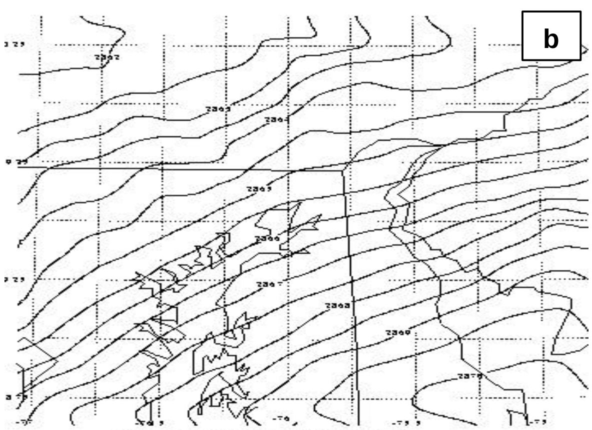

Figure 4. NHMASS simulated a) 2 km 285K absolute vorticity ($s^{-1} \times 10^{-4}$) and b) Montgomery stream function (m^2s^{-2}) for the Wilmington, Delaware case study valid at 2100 UTC 13 January 2000.

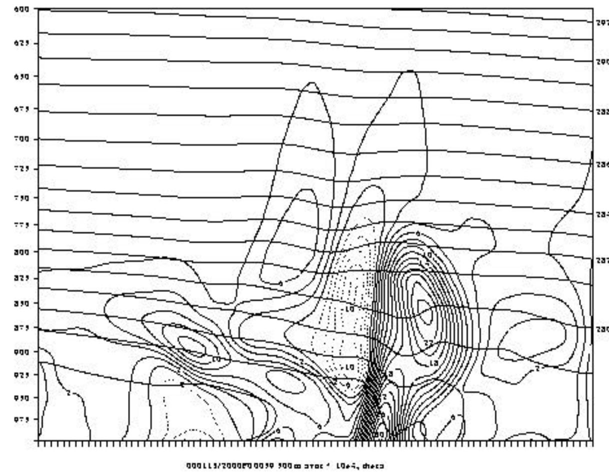

Figure 5. NHMASS simulated 500 m vertical cross section of potential temperature (K) and absolute vorticity ($s^{-1} \times 10^{-4}$) centered on the Wilmington, Delaware case valid at 2100 UTC 13 January 2000.

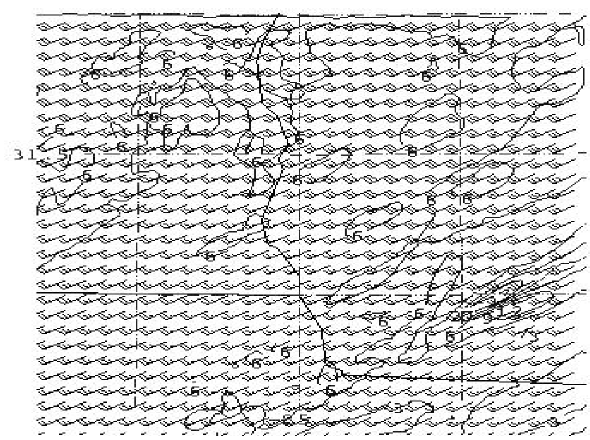

Figure 6. NHMASS simulated 2 km 334K wind barbs (ms^{-1}) and absolute vorticity ($s^{-1} \times 10^{-4}$) for the Valdosta, Georgia case study flight experiment valid at 1845 UTC 14 December 2000.

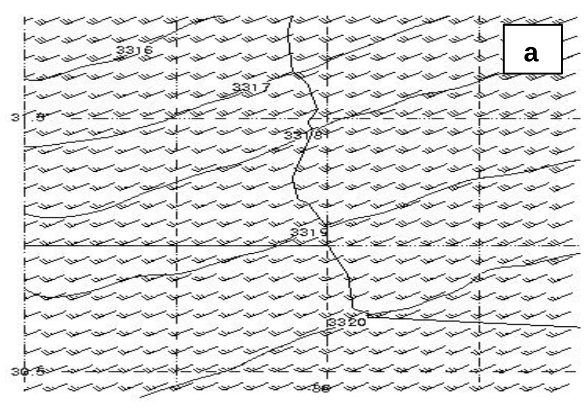

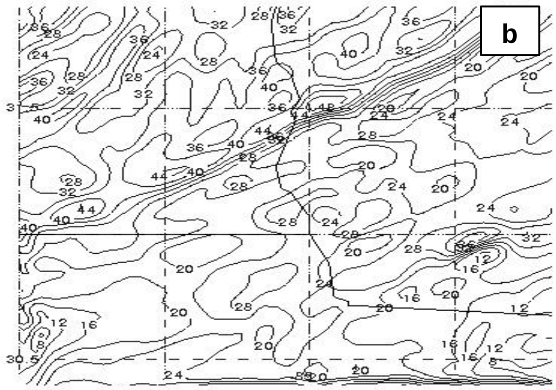

Figure 7a. NHMASS simulated 2 km 334K M (m^2s^{-2}) for the Valdosta, Georgia case study flight experiment valid at 1845 UTC 14 December 2000 and b). NHMASS simulated 2 km 334K gradient of M (ms^{-2} x 10^{-4}) for the Valdosta, Georgia case study flight experiment valid at 1845 UTC 13 January 2000.

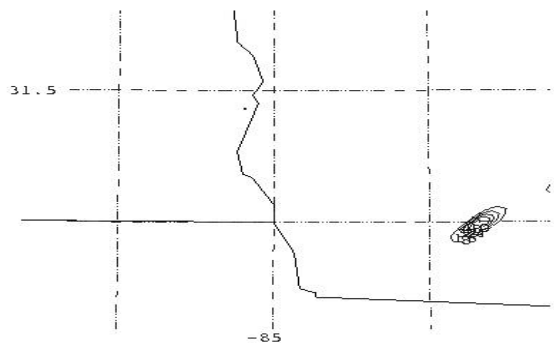

Figure 8. NHMASS simulated 2 km 334K positive values of the cross product of the gradient of M and the gradient of the relative vorticity (s^{-3} x 10^{-8}) for the Valdosta, Georgia case study flight experiment valid at 1845 UTC 14 December 2000.

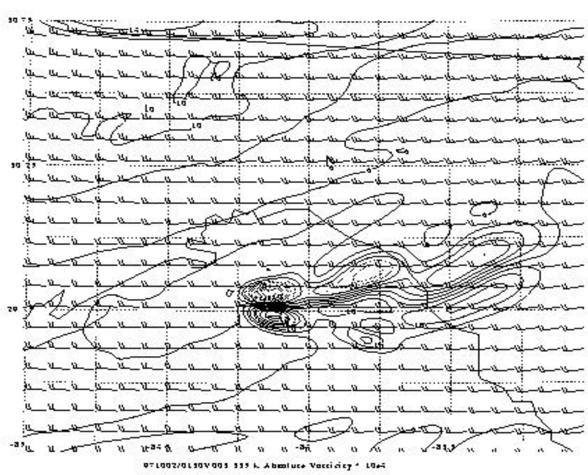

Figure 9. NHMASS simulated 2 km 335K wind barbs (ms^{-1}) and absolute vorticity (s^{-1} x 10^{-4}) for the Cross City, Florida case valid at 0130 UTC 2 October 1997.

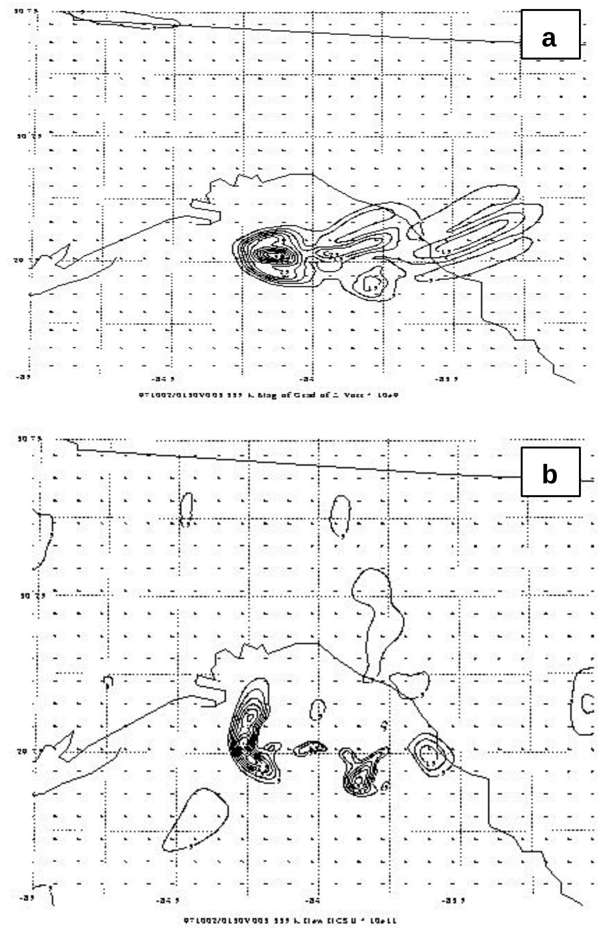

Figure 10. NHMASS simulated 2 km 335K gradient of relative vorticity ($s^{-1}m^{-1}$ x 10^{-4}) for the Cross City, Florida case valid at 0130 UTC 2 October 1997. b) NHMASS simulated 2 km 335K gradient of M (ms^{-2} x 10^{-4}) for the Cross City, Florida case valid at 0130 UTC 2 October 1997.

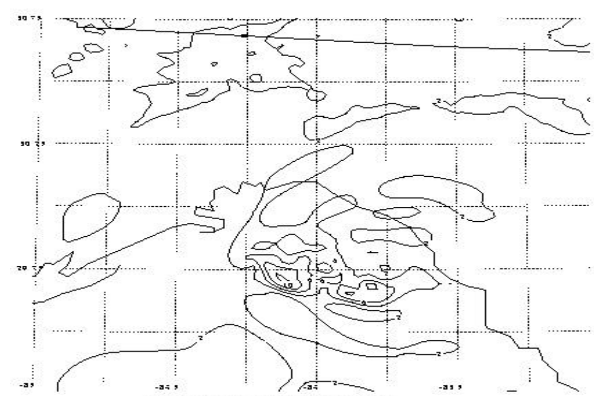

Figure 11. NHMASS simulated 2 km 335K positive values of the cross product of the gradient of M and the gradient of the relative vorticity (s^{-3} x 10^{-8}) for the Cross City, Florida case valid at 0130 UTC 2 October 1997.